Extended Kalman Filter for state-of-charge estimation in electric vehicles battery packs

Florin Ciortea, Corneliu Rusu, Marian Nemes, Cătălin Gatea
Technical University of Cluj-Napoca, Basis of Electronics Department
ciorteaflorin@yahoo.com, corneliu.rusu@bel.utcluj.ro, calin.nemes@gmail.com, cata_gatea@yahoo.com

***Abstract*-Efficacious work of the Li-ion battery (LIB) is strongly influenced by several factors as temperature, nominal voltage, capacity and charge/discharge current rate, determining its health and state-of-charge (SOC). SOC is an indicator mirroring the available charge stored in the battery relative to its maximum capacity when new, resembling the fuel gauge in the conventional, internal combustion engine (ICE) vehicles. As this parameter defines rather a condition than a physical quantity, direct measurement using classical means is not feasible. Hence, one needs to "precisely guess" the actual available charge within the battery, in order to operate the battery pack effectively. Among the many methods employed for estimating the batteries' SOC, the Extended Kalman Filter (EKF) stands out due to its intrinsic predictor-corrector mechanism, which makes the filter insensitive to various modeling deficiencies like poor impromptu initialization or noise. This paper presents a step-by-step design procedure of such a filter, based on a 2nd order Thévenin battery equivalent circuit model (ECM). The high performance of the filter estimator is validated against laboratory measurements.**

I. INTRODUCTION

One of the essential requirements of any battery management systems (BMS) is to assess accurately the available charge within its constituent cells. The consequences of precisely estimating the state-of-charge (SOC) reverberate in many aspects:

- prolonged life expectancy of the battery pack, by avoiding severe damage of the cells on account of overcharging and over-discharging;
- enhanced system reliability, due to deterministic behavior of the estimator;
- optimal design of the battery string, with direct impact on size and weight;
- reduced cost, as a result of optimal engineering.

A simple method to estimate the SOC is to establish a linear relationship between the open circuit voltage (OCV) and the available charge. Unfortunately, this approach is not suitable for dynamic applications due to the long resting times (several hours) required for the OCV settlement after a charge/discharge event. Also, as illustrated in Fig. 1, the OCV of LIB is somewhat flat across a wide range of the SOC, requiring a very accurate measurement (for $LiFePO_4$ chemistry the OCV varies with less than 0.1 V over more than half of the SOC interval). Consequently, the need for precise input data forces the usage of high resolution A/D converters, as to measure the battery terminal voltage with a minimum of 5 mV accuracy [1].

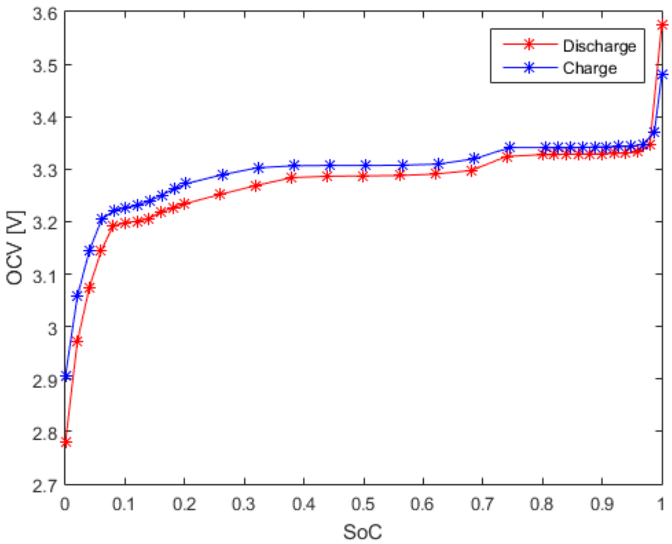

Fig. 1 OCV vs SOC ($LiFePO_4$ cathod after one hour resting period)

Another intuitive and plain means to determine SOC is the Coulomb Counting method, which returns the value of the available charge based on the initial battery loading status and the amount of charge stored or freed afterwards. The equivalent equation is given bellow:

$$SOC(t+\Delta t) = SOC(t) - \frac{1}{C_n} \cdot \int_{t}^{t+\Delta t} \eta \cdot I(t) \cdot dt \qquad (1)$$

where:

- *SOC(t)* represents the battery SOC at initial time *t*;
- C_n is the rated capacity in standard conditions [A·h];
- *I(t)* is the current as a function of time (positive while discharging) [A];
- η is the Coulombic efficiency (unity for discharge).

Erroneous initial state values end up deteriorating the estimation dramatically, while the error introduced by the current sensing elements (measurement off-set and noise) alters the estimation even more (long-term drift) proving the method is ineffective.

An adaptive nonlinear observer and a two-time-scale signal processing scheme for SOC prediction is introduced in [2]. The observer compensates nonlinearity providing better

978-1-5090-4489-4/17/$31.00 ©2017 IEEE

accuracy while the two-time-scale signal processing approach attenuates the effects of measurement noise on SOC assessment. A mixed algorithm combining the best features of the Coulomb counting with a comprehensive LIB model is presented in [3] and analyzed for performance in [4] and [5]. The subsequently explained algorithm is relatively simple and robust with respect to measurement noise and does not require precise SOC initialization.

Each before-mentioned technique claims to provide a more or less precise evaluation of the SOC. Yet, none of them is as cited and unanimously agreed for performance as the Extended Kalman Filter (EKF) method [6]-[10]. The EKF is a nonlinear variation of its straight homonym which congregates a suite of recurrent mathematical expressions continually assessed during system operation. This means that the actual state estimation is computed based only on the *a priori* estimated state and the *a posteriori* running measurements. The extended attribute is due to cyclic linearization process embedded within the basic Kalman Filter (KF) frame. This process brings the nonlinear system near to a linear time-variant one, exhibiting an explicitly time dependent output characteristic. It overcomes the shortcomings of the voltage method and the current integration method due to its inherent predictor-corrector mechanism. However, its estimation is symbiotically dependent on physical models of the processes in question, viz. the battery dynamics. The model includes the unknown parameter (SOC) within its state description; therefore model insubstantiality will introduce estimation errors.

II. EKF IMPLEMENTATION

The EKF implementation is a two step procedure. Firstly, the battery model is developed as to closely mimic the real behavior of the device. This step concludes by generating the state-space equations of the model. The second step maps the previously determined state-space model within the predefined structure of the filter. In addition to the linear version of the filter, the extended variant incorporates a linearization stage in order to make the prediction reliable.

A. The LIB equivalent circuit model

There are several ways to emulate the actual behavior of a battery, from intricate electro-chemical models to more intuitive equivalent circuit models (ECM). The former represents a convenient approach that provides an efficient alternative to dealing with the cumbersome chemistry inside the battery [11]. Basic circuit elements (i.e. voltage sources, resistors and capacitors) are electrically interconnected as to account for the highly nonlinear performance of the LIB.

Fig. 2 illustrates a 2nd order RC battery model containing:

- two RC branches, shaping the transient response of the device;
- a purely ohmic component (R_0), allowing for instant changes in terminal voltage due to the load current;
- a SOC dependant open circuit voltage (OCV) source.

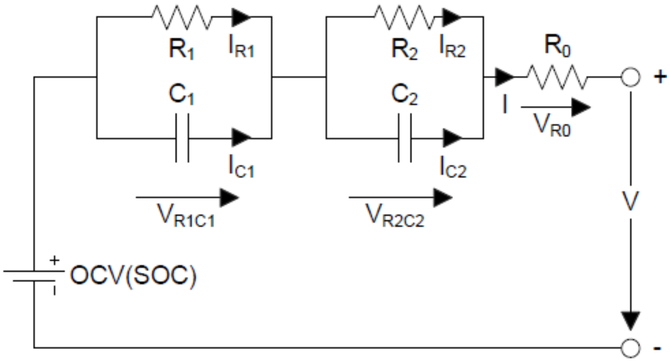

Fig. 2 Second order Thévenin battery model (discharge)

For the sake of brevity, the two RC branches, lumped within the battery model, are behaviorally equated as a rule. This approach suffices as the two circuit meshes are schematically equivalent. Applying charge conservation law at the relevant circuit nodes gives (2):

$$I_{R_i} + I_{C_i} = I \tag{2}$$

The differential voltage across capacitor C_i is determined next:

$$I_{C_i} = C_i \cdot dV_{R_iC_i} / dt \tag{3}$$

$$I_{R_i} = V_{R_iC_i} / R_i \tag{4}$$

$$dV_{R_iC_i} / dt = -V_{R_iC_i} / (R_i \cdot C_i) + I / C_i \tag{5}$$

Finally, the energy conservation law for conservative fields across the main loop is expressed in (6):

$$OCV(SOC) - V = \sum_{i=1}^{n} V_{R_iC_i} + I \cdot R_0 \tag{6}$$

where n is an integer representing the number of RC branches.

The equivalent battery model specific relations are further arranged within a matrix structure representing the state-space equation of the model according to (7):

$$\frac{d}{dt}\begin{bmatrix} SOC \\ V_{R_1C_1} \\ V_{R_2C_2} \end{bmatrix} = M \cdot \begin{bmatrix} SOC \\ V_{R_1C_1} \\ V_{R_2C_2} \end{bmatrix} + N \cdot I \tag{7}$$

where:

$$M = \begin{bmatrix} 1 & 0 & 0 \\ 0 & -1/R_1C_1 & 0 \\ 0 & 0 & -1/R_2C_2 \end{bmatrix}, N = \begin{bmatrix} -1/C_n \\ 1/C_1 \\ 1/C_2 \end{bmatrix}$$

By applying Euler's discretization method the ordinary differential equation (ODE) in (7) becomes:

$$SOC_{k+1} = SOC_k - \Delta t \cdot I_k / C_n \quad (8)$$

$$V_{R_iC_i,k+1} = V_{R_iC_i,k} - \Delta t \cdot V_{R_iC_i,k} / (R_i \cdot C_i) + \Delta t \cdot I_k / C_i \quad (9)$$

where the $k+1$ time index increment refers the immediate upcoming state relative to precedent k, approximated by a piecewise linear curve over a Δt time span.

The practical, time-discrete, state-space equated battery model is disclosed in (10). This one is eventually plugged within the EKF SOC estimation algorithm, next to the terminal voltage measurement equation in (11).

$$\begin{bmatrix} SOC_{k+1} \\ V_{R_1C_1,k+1} \\ V_{R_2C_2,k+1} \end{bmatrix} = M \cdot \begin{bmatrix} SOC_k \\ V_{R_1C_1,k} \\ V_{R_2C_2,k} \end{bmatrix} + N \cdot I_k \quad (10)$$

where:

$$M = \begin{bmatrix} 1 & 0 & 0 \\ 0 & 1-\Delta t/R_1C_1 & 0 \\ 0 & 0 & 1-\Delta t/R_2C_2 \end{bmatrix}, N = \begin{bmatrix} -\Delta t/C_n \\ \Delta t/C_1 \\ \Delta t/C_2 \end{bmatrix}$$

$$V_k = OCV(SOC_k) - \sum_{i=1}^{n} V_{R_iC_i,k} - I_k \cdot R_0 \quad (11)$$

1) ECM parameters variation with SOC

As the ECM parameters vary widely across the SOC interval, accounting for a unique value is inadequate. Fig. 3 illustrates the distribution of the model's parameters as a function of SOC according to [12] and the corresponding fit functions developed following [13] and [14].

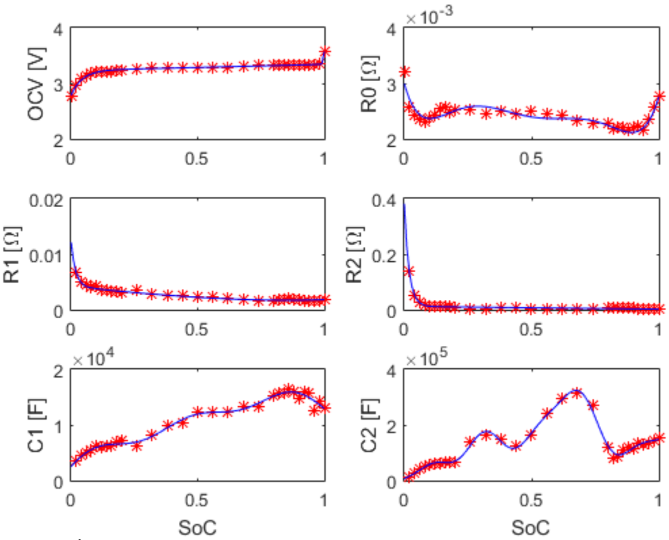

Fig. 3 2nd order battery model parameters fit

The mathematical expressions describing the SOC dependency of the battery model parameters are unfolded in (12)-(17) and will be used later in the filter implementation.

$$\begin{aligned} OCV_d(S) &= a_1 + a_2 \cdot \frac{1}{1+e^{a_3\cdot(S-a_4)}} + \\ &+ a_5 \cdot \frac{1}{1+e^{a_6\cdot(S-a_7)}} + a_8 \cdot \frac{1}{1+e^{a_9\cdot(S-1)}} + \\ &+ a_{10} \cdot \frac{1}{1+e^{a_{11}\cdot S}} + a_{12} \cdot S \end{aligned} \quad (12)$$

$$\begin{aligned} R_{0d}(S) &= b_1 \cdot S^6 + b_2 \cdot S^5 + b_3 \cdot S^4 + \\ &+ b_4 \cdot S^3 + b_5 \cdot S^2 + b_6 \cdot S + b_7 \end{aligned} \quad (13)$$

$$R_{1d}(S) = c_1 \cdot e^{c_2\cdot S} + c_3 + c_4 \cdot S + c_5 \cdot e^{c_6\cdot S} \quad (14)$$

$$R_{2d}(S) = d_1 \cdot e^{d_2\cdot S} + d_3 + d_4 \cdot S \quad (15)$$

$$\begin{aligned} C_{1d}(S) &= e_1 \cdot \sin(e_2 \cdot S + e_3) + \\ &+ e_4 \cdot \sin(e_5 \cdot S + e_6) + e_7 \cdot \sin(e_8 \cdot S + e_9) \end{aligned} \quad (16)$$

$$\begin{aligned} C_{2d}(S) &= f_1 \cdot \sin(f_2 \cdot S + f_3) + \\ &+ f_4 \cdot \sin(f_5 \cdot S + f_6) + f_7 \cdot \sin(f_8 \cdot S + f_9) \end{aligned} \quad (17)$$

where the variable S represents the state-of-charge, the subscript d stands for discharge and the indexed coefficients values are given in Table I:

TABLE I
EQUIVALENT BATTERY MODEL PARAMETERS VALUES

a_1	3.42	b_5	0.1415	e_4	7531
a_2	154.5	b_6	-0.01603	e_5	12.58
a_3	-140.8	b_7	0.002993	e_6	-1.253
a_4	1.051	c_1	0.007915	e_7	7829
a_5	0.05668	c_2	-55.65	e_8	13.18
a_6	-21.15	c_3	0.002328	e_9	1.596
a_7	0.22	c_4	-0.007398	f_1	2.27e+05
a_8	-0.229	c_5	0.001895	f_2	2.834
a_9	167.8	c_6	1.289	f_3	-0.2-74
a_{10}	-0.8151	d_1	0.3696	f_4	-5.349e+04
a_{11}	46.48	d_1	-54.36	f_5	12.76
a_{12}	0.0891	d_3	0.01203	f_6	-3.482
b_1	0.2667	d_4	-0.01	f_7	4.8e+04
b_2	-0.8066	e_1	1.418e+04	f_8	19.53
b_3	0.9391	e_2	1.678	f_9	-5.001
b_4	-0.5249	e_3	0.1305	-	-

2) C_{use} vs. C_n

The usable capacity [A·h] is not necessarily equal to the nominal capacity of the battery, as it varies with both temperature and discharge current. This paper treats only the second influencing factor as the experiments were carried out only at room temperature. In order to determine the relationship between the actual capacity and the discharge current rate the battery was fully charged several times, each time being continuously depleted of charge at different Crates (0.1-C, 0.5-C, 1-C, 2-C and 3-C) until the cut-off voltage limit was reached. The removed charge amount during each discharge cycle was tracked using the Coulomb counter provided by the data acquisition module [12]. Varying the current rate during charging did not pose significant differences concerning the stored charge quantity due to the CC-CV charging mode.

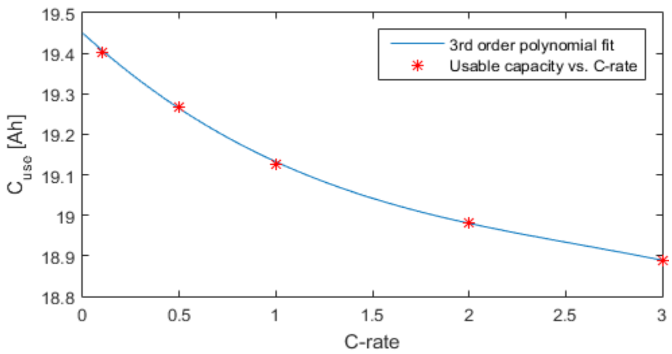

Fig. 4 Polynomial fiting of C_{use}

Fig. 4 pictures the decaying characteristic of the usable capacity with the increasing C-rate. The workable charge gets close to the nominal value for low discharge currents and diminishes nonlinearly as the current rate enlarges. A third order polynomial was required in order to satisfactorily link the experimental data points. The resulted equation is expressed in (18):

$$C_{use} = a_1 \cdot C-r^3 + a_2 \cdot C-r^2 + a_3 \cdot C-r + a_4 \quad (18)$$

where C-r denotes the discharge current rate and the polynomial coefficients values are stated in Table II:

TABLE II
PARAMETERS VALUES FOR C_{USE} FIT

a_1	-0.01753	a_2	0.1355	a_3	-0.4357	a_4	19.45

B. EKF for SOC prediction

The EKF process (19) and measurement (20) models are governed by the nonlinear vector functions, f and g, where x_k is the state vector at time index k, y_k depicts the observation vector, u_k is the control vector and the random variables w_k and v_k represent the uncorrelated, process and measurement, additive zero-mean noises, with covariance matrices Q and R (21), respectively.

$$x_{k+1} = f(x_k, u_k) + w_k \quad (19)$$

$$y_k = g(x_k, u_k) + v_k \quad (20)$$

$$w_k \sim N(0, Q), v_k \sim N(0, R) \quad (21)$$

The differentiable state transition (22) and measurement (23) functions, are linearized about each sample point by Taylor series expansion truncating the higher than second order terms inclusively. The Jacobian matrices of the first order Taylor expansion are mathematically expressed in (26)-(29), where A_k, C_k are the first partial derivatives matrices of f and g with respect to x_k and B_k, D_k are the Jacobian matrices of the same functions with respect to u_k.

$$f(x_k, u_k) = \begin{bmatrix} \overbrace{SOC_k - \frac{\Delta t}{C_{use}} \cdot I_k}^{f_1(x_k, u_k)} \\ \overbrace{V_{R_1C_1,k} - \frac{\Delta t}{R_1 \cdot C_1} \cdot V_{R_1C_1,k} + \frac{\Delta t}{C_1} \cdot I_k}^{f_2(x_k, u_k)} \\ \overbrace{V_{R_2C_2,k} - \frac{\Delta t}{R_2 \cdot C_2} \cdot V_{R_2C_2,k} + \frac{\Delta t}{C_2} \cdot I_k}^{f_3(x_k, u_k)} \end{bmatrix} \quad (22)$$

$$g(x_k, u_k) = \left[OCV_k - V_{R_1C_1,k} - V_{R_2C_2,k} - R_0 \cdot I_k \right] \quad (23)$$

$$x_k = \begin{bmatrix} \overbrace{SOC}^{x_1} & \overbrace{V_{R_1C_1,k}}^{x_2} & \overbrace{V_{R_2C_2,k}}^{x_3} \end{bmatrix} \quad (24)$$

$$u_k = I_k \quad (25)$$

$$A_k = \frac{\partial f(x_k, u_k)}{\partial x_k} = \begin{bmatrix} \frac{\partial f_1}{\partial x_1} & \frac{\partial f_1}{\partial x_2} & \frac{\partial f_1}{\partial x_3} \\ \frac{\partial f_2}{\partial x_1} & \frac{\partial f_2}{\partial x_2} & \frac{\partial f_2}{\partial x_3} \\ \frac{\partial f_3}{\partial x_1} & \frac{\partial f_3}{\partial x_2} & \frac{\partial f_3}{\partial x_3} \end{bmatrix} = \begin{bmatrix} 1 & 0 & 0 \\ 0 & 1 - \Delta t/(C_1 \cdot R_1) & 0 \\ 0 & 0 & 1 - \Delta t/(C_2 \cdot R_2) \end{bmatrix} \quad (26)$$

$$B_k = \frac{\partial f(x_k, u_k)}{\partial u_k} = \begin{bmatrix} \partial f_1/\partial u \\ \partial f_2/\partial u \\ \partial f_3/\partial u \end{bmatrix} = \begin{bmatrix} -\Delta t/C_{use} \\ \Delta t/C_1 \\ \Delta t/C_2 \end{bmatrix} \quad (27)$$

$$C_k = \frac{\partial g(x_k, u_k)}{\partial x_k} = \begin{bmatrix} \partial g/\partial x_1 \\ \partial g/\partial x_2 \\ \partial g/\partial x_3 \end{bmatrix}^T = \begin{bmatrix} \frac{\partial OCV}{\partial SOC} \\ -1 \\ -1 \end{bmatrix}^T \quad (28)$$

$$D_k = \frac{\partial g(x_k, u_k)}{\partial u_k} = \left[\frac{\partial g}{\partial u} \right] = [-R_0] \quad (29)$$

As one can notice, excepting C_k, all the afore-determined Jacobian matrices are fixed. The initial term in C_k represents the first derivative of (12) and is graphically shown in Fig. 5.

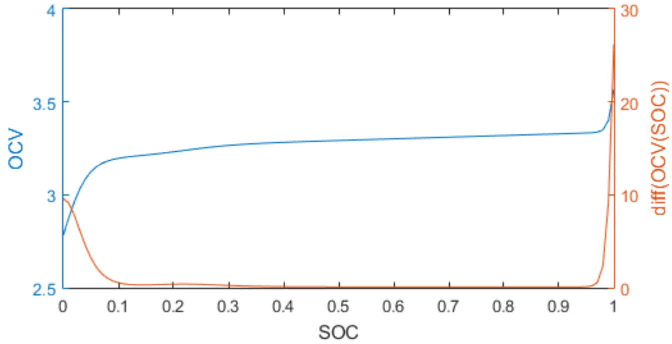

Fig. 5 OCV fit as a function of SOC (12) and its first derivative

The discrete time space form of the practical model after linearization is written in (30) and (31). The two equations depict the process model and the measurement model, respectively.

$$x_{k+1} = A_k \cdot x_k + B_k \cdot u_k + w_k \tag{30}$$

$$y_k = C_k \cdot x_k + D_k \cdot u_k + v_k \tag{31}$$

The EKF starts filtering relying on the initial state and error covariance information available at the first step ($k = 0$):

$$\begin{aligned} x_k^o &= E[x_k] \\ P_k^o &= E\left[\left(x_k - x_k^o\right)\cdot\left(x_k - x_k^o\right)^T\right] \end{aligned} \tag{32}$$

P_k is the prediction error covariance matrix associated to x_k approximation, containing information about the uncertainty on estimated value of x at time index k.

Over the time update step, the filter predicts the state value (33) and error covariance matrix (34), according to the process model and based on revised-by-measurement values during the previous time index ($x^p_{k+1} \leftarrow x^o_k$). As this is a precursory stage of the filtering process the resulted terms are appointed as inferential data and indicated by superscript "*p – predicted*", in terms of notation.

$$x_{k+1}^p = f\left(x_k^o, u_k\right) = A_k \cdot x_k^o + B_k \cdot u_k \tag{33}$$

$$P_{k+1}^p = A_k \cdot P_k^o \cdot A_k^T + Q \tag{34}$$

During the correction or measurement update the filter gets feedback from the measurement unit to submit an improved state denoted with the superscript "*o – optimized*" or *original* estimate for $k = 0$ (36). The kernel of the KF algorithm is represented by the Kalman gain matrix derivation, K in (35), which binds the two filtering steps by moderating the prediction process. The effective correction term or "innovation" is represented by the parenthesis content in (36), which equates the difference between the actual measurement (y) and the estimation of the measurement (y^p) at time step $k+1$. The accuracy of the filter increases inversely with the correction term value. The Kalman gain is used to determine how much of the new measurement to use to update the new estimate. Over time, typically, the size of the Kalman gain will dwindle, meaning that the filter converges to the true value and the estimates are becoming more accurate.

$$K_{k+1} = P_{k+1}^p \cdot C_{k+1}^T \cdot \left(C_{k+1} \cdot P_{k+1}^p \cdot C_{k+1}^T + R\right)^{-1} \tag{35}$$

$$x_{k+1}^o = x_{k+1}^p + K_{k+1} \cdot \left[y_{k+1} - \overbrace{\left(C_{k+1} \cdot x_{k+1}^p + D_{k+1} \cdot u_{k+1}\right)}^{y_{k+1}^p = g\left(x_{k+1}^p, u_{k+1}\right)} \right] \tag{36}$$

$$P_{k+1}^o = \left(I - K_{k+1} \cdot C_{k+1}\right) \cdot P_{k+1}^p \tag{37}$$

III. Running the EKF

The initial state vector accounted for a half depleted battery and no voltage drop across the two RC branches (chemical equilibrium), $x^o_0 = [0.5 \;\; 0 \;\; 0]^T$. Also, the initial error covariance matrix was selected as $P^o_0 = diag[10, 0.01, 0.01]$.

The Q matrix is a rather holistic parameter which lumps the overall modeling errors (unknown errors inclusively). Large values of Q indicate that the chosen model does a bad job in predicting the process. On the other hand, R determines how much information from the measurement is used. A small R means that the measurements are close to reality. For this application $Q = diag[1e\text{-}05, 1e\text{-}03, 1e\text{-}03]$ and $R = [0.1]$ were empirically determined.

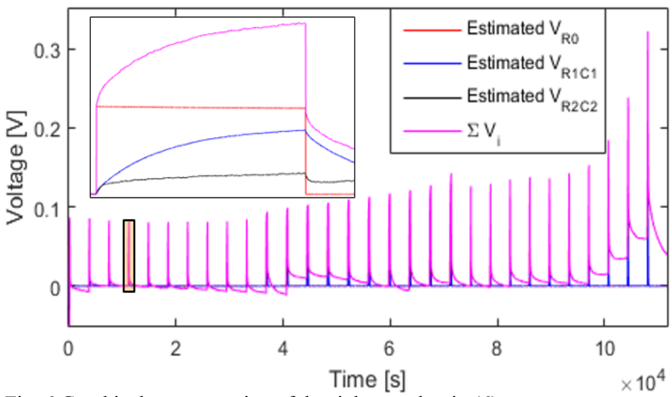

Fig. 6 Graphical representation of the right member in (6)

Fig. 6 plots the estimated, individual and cumulated, voltage drops across the battery model branches.

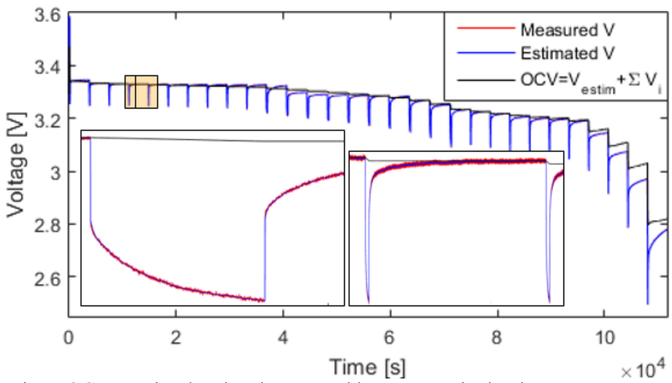

Fig. 7 OCV vs. simulated and measured battery terminal voltage

Fig. 7 illustrates the simulated terminal voltage, overlaying the measured one, during a pulsed discharge pattern (1-C: 10×2% of SOC → 10×6% of SOC → 10×2% of SOC). The black colored signal approaching the tips of the terminal voltage rest intervals represents the estimated OCV.

Fig. 8 highlights the rate of convergence of the simulated terminal voltage and SOC to their measured peers. Although once "clamped", the battery terminal voltage follows closely the real signal over the entire discharge timeline, the estimated SOC slightly loses track with time. This is due to process model inconsistencies, suppression of higher order terms of the Taylor series expansion and mainly due to the current integration error (drift error). The maximum estimation error was close to 2% whilst the RMS error value approached 0.75% (the error calculation was done without considering the period of convergence).

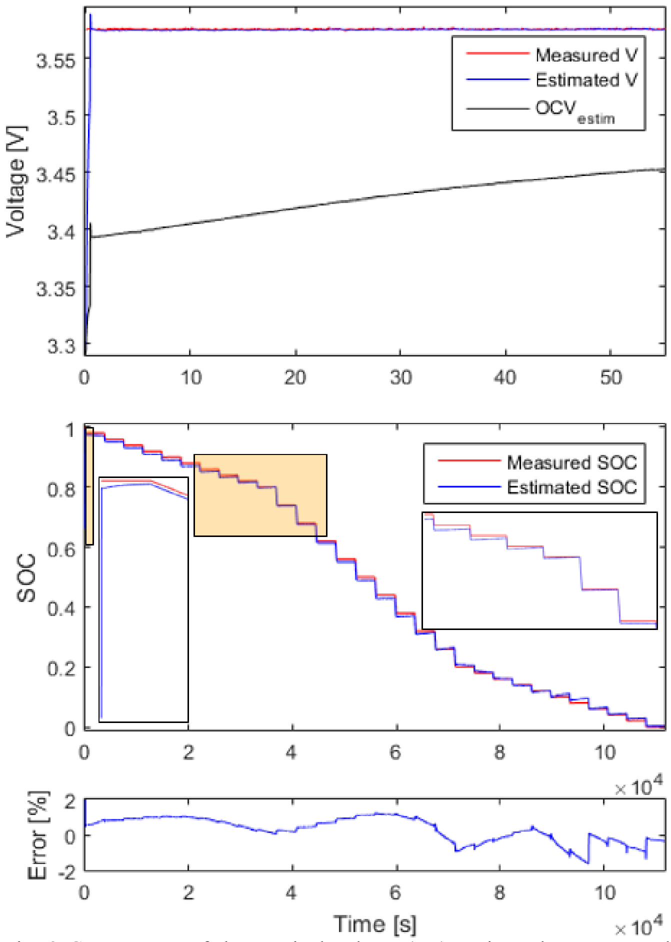

Fig. 8 Convergence of the terminal voltage (top), estimated vs. measured SOC (middle), SOC estimation error (bottom)

The same EKF kernel was used, with constant electrical parameters: $R_0 = 2.4$ mΩ, $R_1 = 2.3$ mΩ, $R_2 = 3.9$ mΩ, $C_1 = 11.326$ F, $C_2 = 196816$ F. The parameters were chosen based on an average value in the 20-80% SOC interval. This resulted in a RMS error of 2.5%, with a peak at 6%. Notable is the reduction in simulation time for constant parameters, at halve duration, but with a 3 times increase in error.

IV. CONCLUSIONS

A research on the topic of SOC estimation for LIB was done, targeting implementation in a battery management system. The disadvantages of various simple SOC estimation methods guided the research towards complex estimation algorithms such as the EKF. An appropriate ECM discharge model was chosen; the state-space equations were written and linearized in order to fit the EKF algorithm. An implementation was written in Matlab, and then tested against measurement data for validation. The estimation accuracy and convergence performance have been presented in this paper. Due to the usage of variable model parameters and an appropriately accurate ECM, results are better than a similar but constant parameter estimator. This approach is valid for a charge sequence, while a charge/discharge interleaved pattern would require a more sophisticated implementation that will make the subject of future work.

REFERENCES

[1] M. Kultgen, "Managing high-voltage lithium-ion batteries in HEVs," unpuplished. *Linear Tehnology Corp*, April 2009. [Online]. Available: http://cds.linear.com/docs/en/article/EDN%20M%20Kultgen%20LTC6802.pdf

[2] L. Liu et al., "Integrated System Identification and State-of-Charge Estimation of Battery Systems," *IEEE Transactions on Enegry Conversion*, vol. 28, pp. 12-23, October 2012.

[3] F. Codeca, S. M. Savaresi and G. Rizzoni, "On battery State of Charge estimation: A new mixed algorithm," *17th IEEE International Conf. on Control Applications*, pp. 102-107, September 2008.

[4] S. M. Savaresi, V. Manzoni and F. Codeca, "The mix estimation algorithm for state-of-charge estimator analysis of the sensitivity to model errors," *2nd Dynamic Systems and Control Conf.*, pp. 1-8, October 2009.

[5] F. Codeca, S. M. Savaresi and V. Manzoni, "The mix estimation algorithm for battery State-of-Charge estimator – Analysis of the sensitivity to measurement errors," *48th IEEE Conf. on Decision and Control*, pp. 8083-8088, January 2010.

[6] G. L. Plett, "Extended Kalman filtering for battery management systems of LiPB-based HEV battery packs Part 1. Background," *J. of Power Sources*, vol. 134, pp. 252-261, August 2004.

[7] G. L. Plett, "Extended Kalman filtering for battery management systems of LiPB-based HEV battery packs Part 3. State and parameter estimation," *J. of Power Sources*, vol. 134, pp. 277-292, August 2004.

[8] H. Dai, Z. Sun and X. Wei, "Online SOC Estimation of High-power Lithium-ion Batteries Used on HEVs," *IEEE International Conf. on Vehicular Electronics and Safety*, pp. 342-347, June 2007.

[9] Z. W. Zhu, D. Liu, Y. Rong and J. Sun, "SOC EKF Estimation Based on a Second-order $LiFePO_4$ Battery Model," *TELKOMNIKA*, vol. 11, pp. 4208-4213, August 2013.

[10] L. W. Yao, W. A/I. Prayun, J. A. Aziz and T. Sutikno, "Battery State of Charge Estimation with Extended Kalman Filter Using Third Order Thevenin Model," *TELKOMNIKA*, vol. 13, pp. 401-412, June 2015.

[11] A. A.-H. Hussein and I. Batarseh, "An overview of generic battery models," *2011 IEEE/PES General Meeting*, July 2011.

[12] F. Ciortea, S. Hintea, C. Gatea and M. Nemes, "Measurement method and parametric modelling of $LiFePO_4$ cell for SOC estimation in EVs," unpublished.

[13] L. Lam, P. Bauer and E. Kelder, "A Practical Circuit-based Model for Li-ion Battery Cells in Electric Vehicle Applications," *33rd IEEE International Telecom. Energy Conf.*, December 2011.

[14] C. Weng, J. Sun and H. Peng, "An Open-Circuit-Voltage Model of Lithium-Ion Batteries for Effective Incremental Capacity Analysis," *Proceedings of the ASME Dynamic Systems and Control Conf.*, pp. 1-8, October 2013